

## Peripheral hyperstimulation alters site of disease onset and course in SOD1 rats

Angelo C. Lepore<sup>a</sup>, Christopher Tolmie<sup>a</sup>, John O'Donnell<sup>a</sup>, Megan C. Wright<sup>a</sup>, Christine Dejea<sup>a</sup>, Britta Rauck<sup>a</sup>, Ahmet Hoke<sup>a</sup>, Anthony R. Ignagni<sup>b</sup>, Raymond P. Onders<sup>c</sup>, Nicholas J. Maragakis<sup>a,\*</sup>

<sup>a</sup> Department of Neurology, The Johns Hopkins University School of Medicine, Baltimore, MD, USA

<sup>b</sup> Synapse Biomedical Inc., Cleveland, OH, USA

<sup>c</sup> Department of Surgery, Case Medical Center of University Hospitals and Case Western Reserve University, Cleveland, OH, USA

### ARTICLE INFO

#### Article history:

Received 10 November 2009

Revised 1 March 2010

Accepted 29 March 2010

Available online 8 April 2010

#### Keywords:

Motor neuron

Neurodegeneration

ALS

Amyotrophic lateral sclerosis

SOD1

Phrenic nerve

Diaphragm

Diaphragm pacing

Diaphragm stimulation

Respiratory

Disease onset

Environment

### ABSTRACT

In amyotrophic lateral sclerosis (ALS), the exogenous temporal triggers that result in initial motor neuron death are not understood. Overactivation and consequent accelerated loss of vulnerable motor neurons is one theory of disease initiation. The vulnerability of motor neurons in response to chronic peripheral nerve hyperstimulation was tested in the SOD1<sup>G93A</sup> rat model of ALS. A novel in vivo technique for peripheral phrenic nerve stimulation was developed via intra-diaphragm muscle electrode implantation at the phrenic motor endpoint. Chronic bilateral phrenic nerve hyperstimulation in SOD1<sup>G93A</sup> rats accelerated disease progression, including shortened lifespan, hastened motor neuron loss and increased denervation at diaphragm neuromuscular junctions. Hyperstimulation also resulted in focal decline in adjacent forelimb function. These results show that peripheral phrenic nerve hyperstimulation accelerates cell death of vulnerable spinal motor neurons, modifies both temporal and anatomical onset of disease, and leads to involvement of disease in adjacent anatomical regions in this ALS model.

Published by Elsevier Inc.

### Introduction

Potential exogenous triggers or risk factors for motor neuron degeneration and the development of amyotrophic lateral sclerosis (ALS) have been hypothesized, including infectious etiologies such as viruses (Mattson, 2004), toxic or heavy metal exposures (Sutedja et al., 2008b), central nervous system or peripheral nerve trauma (Mitsumoto et al., 1998), occupation (Sutedja et al., 2008a), exercise and body habitus (Chen et al., 2008), amongst others. More recently, the hunt for disease modifying genes has also been undertaken (Ravits and Traynor, 2008). However, little is known about the factors that influence the anatomical site of disease onset in ALS. Why does disease start with limb onset in one patient, while it begins with speech, swallowing or breathing problems in another? It is also not appreciated which factors play a role in the anatomical progression of disease to adjacent regions of the neuraxis. For example, patients with weakness in one leg generally develop weakness in the other leg prior

to the development of speech or swallowing abnormalities. This pattern is also manifested in the caudal-to-rostral disease progression observed in mutant human SOD1-expressing transgenic rodent models.

The vast majority of ALS cases are sporadic, while approximately 10% are familial. Twenty percent of familial cases are linked to various point mutations in the Cu/Zn superoxide dismutase 1 (SOD1) gene on chromosome 21 (Rosen et al., 1993). Transgenic mice (Bruijn et al., 1997; Gurney et al., 1994; Wong et al., 1995) and rats (Howland et al., 2002; Matsumoto et al., 2006; Nagai et al., 2001) carrying mutant human SOD1 genes (G93A, G37R, G86R, G85R) have been generated, and, despite the existence of other animal models of motor neuron loss, are currently the most highly used models of the disease.

ALS patients ultimately succumb to disease approximately 2–5 years following diagnosis because of respiratory compromise due to loss of phrenic motor neuron innervation of the diaphragm. Furthermore, the extent of respiratory involvement has been reported as a major prognostic factor (Haverkamp et al., 1995). Interventions targeting respiratory function have resulted in impressive, albeit incomplete, efficacy on ALS patient survival (Lo Coco et al., 2006). We have also shown cervical motor neuron loss, phrenic nerve axonal loss, diaphragm atrophy and progressive reduction of phrenic nerve compound muscle action potential amplitudes in SOD1<sup>G93A</sup> rats

\* Corresponding author. Department of Neurology, The Johns Hopkins School of Medicine, John G. Rangos Bldg., 855 N. Wolfe St., Room 248, Baltimore, MD 21205, USA. Fax: +1 410 502 5459.

E-mail address: [nmaragak@jhmi.edu](mailto:nmaragak@jhmi.edu) (N.J. Maragakis).

Available online on ScienceDirect ([www.sciencedirect.com](http://www.sciencedirect.com)).

(Llado et al., 2006). These results demonstrate a vulnerability of phrenic motor neurons in SOD1<sup>G93A</sup> rats similar to human disease, and demonstrate that decline in respiratory function also plays a central role in disease progression in the rat model of ALS.

By targeting respiratory function in the SOD1<sup>G93A</sup> rat, we have developed a model that influences the site of disease onset, the temporal course of the disease, and results in the anatomical involvement of disease in anatomically adjacent regions. Specifically, we have developed a novel *in vivo* technique for chronic bilateral phrenic nerve stimulation in the SOD1<sup>G93A</sup> rat via intra-diaphragm muscle electrode implantation at phrenic nerve motor endpoints. By hyperstimulating this nerve–muscle connection, we can induce early onset of respiratory dysfunction, symptoms which normally are not observed in the SOD1<sup>G93A</sup> rat until very late in the disease course. Interestingly, these abnormalities also resulted in development of forelimb weakness prior to any hindlimb symptoms, a process that is different from the normal caudal-to-rostral disease course in this model.

This paradigm has several unique features: 1) It regionally activates a defined population of motor neurons (phrenic); 2) It maintains the integrity of the motor unit (no axotomy or traumatic injury is required); 3) It allows for the study of the most clinically relevant aspect of human ALS biology (diaphragm and respiratory function); 4) It is reproducible; 5) It allows for examination of the effects of peripheral nervous system activity/overactivity on central nervous system biology; 6) It is a novel approach for the study of a focally restricted process in a well-studied ALS animal model with an identical mutation and thus a more homogenous neurodegenerative biology.

## Materials and methods

### Animal models

#### SOD1<sup>G93A</sup> rats

Transgenic rats carrying the human SOD1 gene with the G93A mutation were used (Howland et al., 2002). Male and female rats were obtained from Taconic, and maintained as an in-house colony. Typically, untreated SOD1<sup>G93A</sup> mutants first develop hindlimb disease onset, followed by the development of forelimb onset with subsequent progression to endstage, as has been described previously (Howland et al., 2002; Lepore et al., 2008). For all studies, equal numbers of males and females were included in all groups, and animals from the same litter were distributed amongst groups. In addition, age-matched wild-type (WT) Sprague-Dawley rats from Taconic were also used.

#### Care and treatment of animals

The care and treatment of animals in all procedures was conducted in strict accordance with the guidelines set by the European Communities Council Directive (November 24th, 1986), the NIH Guide for the Care and Use of Laboratory Animals, the Guidelines for the Use of Animals in Neuroscience Research and the Johns Hopkins University IACUC, and measures were taken to minimize any potential pain or animal discomfort. Rats were housed at standard temperature (21 °C) and in a light controlled environment with *ad libitum* access to the food and water, and were maintained in racks of ventilated cages located in the same room. In order to avoid dehydration, Aqua-Jel packs were provided when animals started to show disease symptoms.

#### Electrode stimulation

##### Electrode implantation

WT and SOD1<sup>G93A</sup> rats (85–90 days old) received intraperitoneal injections of anaesthetic cocktail [acepromazine maleate (0.7 mg/kg; Fermenta Animal Health, Kansas City, MO), ketamine (95 mg/kg; Fort

Dodge Animal Health; Fort Dodge, IA), and xylazine (10 mg/kg; Bayer, Shawnee Mission, KS)]. A laparotomy was performed to access the posterior surface of the diaphragm, and stimulating electrodes were bilaterally implanted into the center of both hemi-diaphragms to achieve phrenic nerve motor endpoint activation upon external stimulation. By placing the electrodes in different parts of the diaphragm intraoperatively and examining contraction during stimulation, we identified that optimal full diaphragm muscle contractions can be obtained in the adult rat by placing electrodes centrally in the hemi-diaphragm (Fig. 1A). Electrode wires were fed out of the abdomen, and were tunneled subcutaneously towards the back of the animal, just posterior to the base of the skull. The ends of wires were secured via 4-0 suture, and gold sockets were attached to the ends of the wires for daily connection to the external stimulator. In addition, anodes were placed subcutaneously in the back of the animal. All WT and SOD1<sup>G93A</sup> rats were implanted with the full array of electrodes, regardless of whether the animal was part of the stimulated or unstimulated group. Those animals referred to as “unstimulated” underwent the surgical implantation of electrodes and had electrodes in place for the duration of the study. All incisions were closed with 4-0 suture, and animals were placed on a circulating-H<sub>2</sub>O heating pad and were closely monitored for 24 h post-surgery.

#### Stimulation paradigm

Three stimulation paradigms were conducted: 1) SOD1<sup>G93A</sup> rats with high stimulation parameters; 2) SOD1<sup>G93A</sup> rats with low stimulation parameters; 3) WT rats with high stimulation parameters. Except for preliminary experiments (see Results section), all rats received 2 h of continuous stimulation 5 days per week. Stimulation began for all animals at 90 days of age, and stimulation was always conducted on awake, freely behaving animals that were restricted only to their home cage. All SOD1<sup>G93A</sup> rats continued to receive stimulation until disease endstage, while WT rats received stimulation for 8 weeks, and were subsequently sacrificed. External stimulators were attached to the ends of the 2 stimulating electrodes and to the anode, and animals were constantly monitored during the 2 h period of stimulation to prevent detachment of electrodes from the stimulator. Refer to Table 1 for an outline of the study design and numbers and types of animals used for each experiment.

The stimulus was presented through single helix wound stainless steel electrodes with 4.0 mm of exposed length and 5.0 mm<sup>2</sup> of surface area. High stimulation parameters consisted of stimulation delivered at the respiratory rate of 15.0 bursts/min, with stimulus burst duration of 0.8 s, 20.0  $\mu$ s pulse duration, 5.0 mAmp amplitude and an intra-burst frequency of 33.0 Hz. The delivered charge density on a per pulse basis was 0.02  $\mu$ C/mm<sup>2</sup>. With these stimulation parameters, we intentionally hyperstimulated the phrenic nerve at the motor endpoint. Low stimulation parameters consisted of stimulation delivery at the respiratory rate of 15.0 bursts/min, with a 1.0 mAmp amplitude, 10.0  $\mu$ s pulse width (with no ramping) and 12.0 Hz pulse frequency. All variables (including electrodes and anodes, surgical implantation) were the same between high and low stimulation experiments, except for the parameters delivered by the stimulator.

#### Behavioral analysis

Animal weighing and grip strength measurements were conducted starting 1 week post-electrode implantation. Weighing was conducted once per week until endstage, while grip strength measurements were only conducted on specific days (see Results section).

##### Hindlimb and forelimb grip strength

Hind- and forelimb muscle grip strengths were separately determined using a “Grip Strength Meter” (DFIS-2 Series Digital

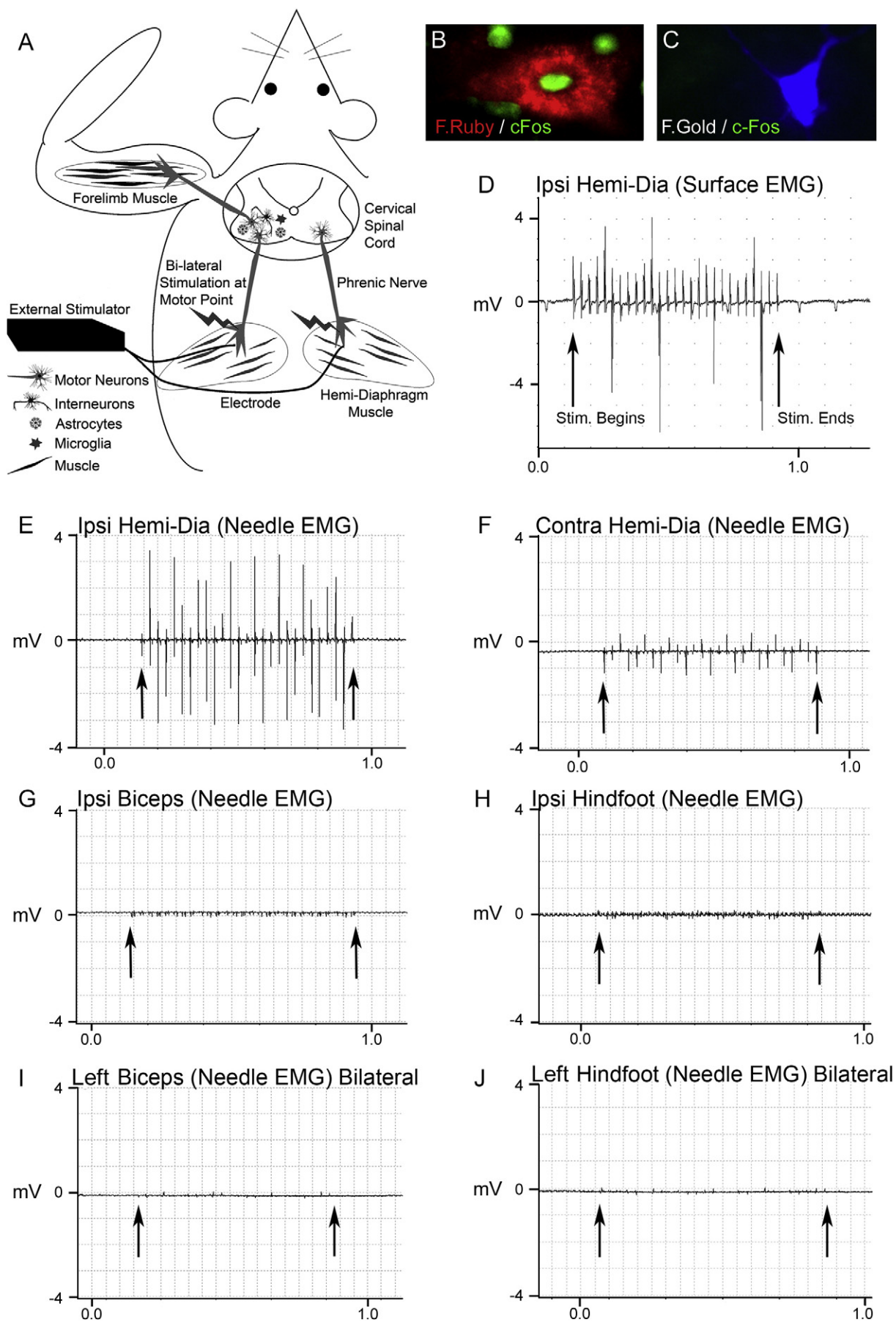


**Table 1**  
Experimental cohort.

Rat type	Sex	Number of rats	Stimulation duration	Surgery/ implant	Stimulation	Parameters	Analysis
Wild-type	M/F	4	8 weeks: start at 90 days	Yes	High stimulation	Varied	Development and validation of technique
SOD1 <sup>G93A</sup>	M/F	6	8 weeks: start at 90 days	Yes	High stimulation	Varied	Development and validation of technique
SOD1 <sup>G93A</sup>	M/F	3	Acute stim at 90 days	Yes	High stimulation	Acute stimulation	Needle and Surface EMGs, c-Fos staining
SOD1 <sup>G93A</sup>	M/F	7	90 days – endstage	Yes	High stimulation	2 h/day 5 days/week	Weight, grip strength, survival, CMAPs at 126 and 138 days of age, motor neuron counts at endstage
SOD1 <sup>G93A</sup>	M/F	7	Unstim	Yes	Unstim (High)	NA	Weight, grip strength, survival, CMAPs at 126 and 138 days of age, motor neuron counts at endstage
SOD1 <sup>G93A</sup>	F	3	90–146 days	Yes	High stimulation	2 h/day 5 days/week	Retrograde axonal tracing, Iba1, NMJ
SOD1 <sup>G93A</sup>	F	3	90–146 days	Yes	Unstim (High)	NA	Retrograde axonal tracing, Iba1, NMJ
Wild-Type	M/F	4	90–146 days	Yes	High stimulation	2 h/day 5 days/week	Weight, grip strength, CMAPs at 146 days of age, motor neuron counts at 146 days of age, retrograde axonal tracing, Iba1, NMJ
Wild-Type	M/F	4	90–146 days	Yes	Unstim (High)	NA	Weight, grip strength, CMAPs at 146 days of age, motor neuron counts at 146 days of age, retrograde axonal tracing, Iba1, NMJ
SOD1 <sup>G93A</sup>	M/F	4	90 days – endstage	Yes	Low stimulation	2 h/day 5 days/week	Weight, grip strength, survival, CMAPs at 111 days of age, motor neuron counts at endstage
SOD1 <sup>G93A</sup>	M/F	5	Unstim	Yes	Unstim (Low)	NA	Weight, grip strength, survival, CMAPs at 111 days of age, motor neuron counts at endstage

Force Gauge; Columbus Instruments, OH) (Lepore et al., 2008). Grip strength testing was performed by allowing the animals to grasp a thin bar attached to the force gauge. This was followed by pulling the animal away from the gauge until the hind- or forelimbs released the bar. This provides a value for the force of maximal grip strength. The force measurements were recorded in three separate trials, and the averages were used in analyses.

#### Survival/endstage analysis

To determine disease endstage in a reliable and ethical fashion, an artificial endpoint was used for all SOD1<sup>G93A</sup> mutant rats (Lepore et al., 2008). Endstage was defined by the inability of rats to right themselves within 30 s when placed on their sides. The moribund rats were scored as “dead”, and were subsequently euthanized.

#### Compound muscle action potential (CMAP) recordings

Under anesthesia, phrenic nerve conduction studies (Llado et al., 2006) were performed with stimulation (0.5 ms single stimulus; 1.0 Hz supramaximal pulses) at the neck via near nerve needle electrodes placed 0.5 cm apart along the phrenic nerve. Recording was obtained via a surface strip along the costal margin, and CMAP amplitude was measured baseline to peak. Recordings across the nerve segment were made using an ADI Powerlab 8SP stimulator and BioAMP amplifier (Powerlab), followed by computer assisted data

analysis (Scope 3.5.6; ADI). Distal motor latency of evoked potentials includes duration of nerve conduction between stimulating and recording electrodes plus time of synaptic transmission.

#### Histological analysis

##### Tissue processing

SOD1<sup>G93A</sup> were sacrificed during the course of disease for immunohistochemistry and tracer analysis or at disease endstage for total cervical motor neuron counts. WT rats were sacrificed at either 146 days of age for immunohistochemistry and motor neuron counts. Animals were transcardially perfused with 0.3% saline, followed by ice-cold 4% paraformaldehyde (Fisher Scientific; Pittsburgh, PA). Spinal cords were removed from the animal, followed by preparation of C4–C6 and L4–L5 spinal cord segments by: 1) cryoprotection in 30% sucrose (Fisher)/0.1 M phosphate buffer at 4 °C for 3 days for immunohistochemistry; 2) washing in 0.1 M phosphate buffer, followed by paraffin-embedding, for motor neuron counts. For immunohistochemistry, tissue was embedded in OCT (Fisher), fast frozen with dry ice, and stored at –80 °C until processed. Spinal cord tissue blocks were cut in the sagittal or transverse planes at 8 µm or 20 µm thicknesses. Sections were collected on glass slides and stored at –20 °C until analyzed. Subsets of spinal cord slices were collected in PBS for free-floating histochemistry.

**Fig. 1.** Phrenic nerve hyperstimulation: technique development in SOD1<sup>G93A</sup> rats. The diagram illustrates the phrenic nerve motor endpoint stimulation technique (A). Stimulating electrodes were bilaterally implanted into the center of both hemi-diaphragm muscles to achieve phrenic nerve activation upon external stimulation. Even though placed directly into muscle, the electrode ends were positioned near the phrenic nerve motor endpoints to allow for stimulation of the phrenic nerve (stimulation/contraction is unsuccessful if there is not phrenic nerve innervation of the diaphragm). The stimulator is found externally, and the ends of the 2 electrodes are connected to the stimulator each day during stimulation, while the animal is awake and freely behaving. Motor neurons innervating the diaphragm originate in the cervical spinal cord, in regions where forelimb motor neurons also reside. This paradigm allows for the study of focal effects on the peripheral nervous system (muscle and nerve), as well as central nervous system effects on motor neurons, astrocytes, and microglia—all key cell types in mutant SOD1-mediated disease (A). Following bilateral phrenic nerve stimulation, c-Fos expression was detected in fluororuby retrogradely labeled phrenic motor neurons (B), but not in fluorogold-labeled forelimb motor neurons (C), suggesting that phrenic nerve stimulation activated phrenic motor neurons, but not forelimb motor neurons. To also examine whether external diaphragm stimulation resulted in ectopic stimulation of other motor neuron/muscle groups (besides phrenic nerve/diaphragm), a comprehensive series of intramuscular needle EMG and muscle surface EMG recordings were obtained during unilateral phrenic nerve stimulation of SOD1<sup>G93A</sup> rats. Stimulation resulted in consistent surface electrical responses in the ipsilateral diaphragm lasting the duration of the programmed stimulus duration (D). Robust intramuscular electrical activity (~3.5 mV) was obtained in the ipsilateral hemi-diaphragm (E) with needle EMG recordings, while a smaller response (~1.0 mV) was also noted in the hemi-diaphragm contralateral to stimulation (F). On the contrary, significant electrical responses during phrenic nerve stimulation were not found with intramuscular needle EMG recordings in the ipsilateral biceps (G) or ipsilateral hindfoot (H). Needle EMG recordings were also conducted in the left biceps (I) and left hindfoot (J) during bilateral phrenic nerve stimulation, and significant electrical activity was not observed. Arrows denote beginning and end of stimulation.



### Immunohistochemistry

GFAP (Chemicon) was used to identify astrocytes, and Iba1 (Wako) was used to detect microglia. c-Fos (AdSerotec) was used to detect activated motor neurons. Samples were incubated for 2 h at room temperature with goat anti-mouse and goat anti-rabbit secondary antibodies (1:200; Jackson, West Grove, PA) conjugated to rhodamine or FITC. Samples were counterstained with DAPI (1:1000; Sigma) to identify nuclei, and cover-slipped with anti-fade mounting media (Fluoromount, CN Biosciences; La Jolla, CA). Slides were subsequently stored at 4 °C. Images were acquired on either a Zeiss fluorescence microscope using a Photometric Sensys KAF-1400 CCD camera (Roper Scientific; Trenton, NJ) or on a Zeiss laser confocal microscope. Images were analyzed using either Metamorph or Zeiss confocal software. Adobe Photoshop 7.0 (Adobe, San Jose, CA) was used to prepare figures.

### Motor neuron survival

The cervical (C4–C6) spinal cord from endstage animals was serially sectioned (14 µm), dehydrated in a graded series of alcohol solutions, embedded in paraffin, and stained with cresyl violet to quantify motor neuron numbers. Motor neurons were counted in every 7th section at 20× magnification in order to avoid repetitive counting. Only motor neurons with a clearly identifiable nucleus and nucleolus, a cell soma over 100 µm<sup>2</sup> and located within the ventral horn were counted at a 200-fold magnification (Llado et al., 2006).

### Neuromuscular junction analysis

Following electrode implantation, three groups of rats were sacrificed at the same age (following 9 weeks of stimulation) for neuromuscular junction analysis: stimulated wild-type, unstimulated SOD1<sup>G93A</sup>, and stimulated SOD1<sup>G93A</sup>. A group of unstimulated SOD1<sup>G93A</sup> rats was also analyzed at disease endstage. One hemi-diaphragm muscle was dissected from each animal for whole-mount immunohistochemistry (Wright et al., 2007). Muscle was stretched, pinned down to Sylgard (Fisher) media, and extensively cleaned to remove any connective tissue to allow for antibody penetration. Motor axons and their terminals were labeled with SMI-312R (Covance) and SV2-s (DSHB), respectively, and both antibody labelings were detected with FITC anti-mouse IgG secondary (Invitrogen). Post-synaptic acetylcholine receptors were labeled with Alexa Fluor 647-conjugated alpha-bungarotoxin (Invitrogen). Labeled muscles were analyzed for total numbers of NMJs, fully innervated NMJs, partially denervated NMJs, completely denervated NMJs, NMJs with terminal sprouting, NMJs with axonal sprouting/partial reinnervation.

### Fluorescent tracer injections and analysis

Fluororuby (dextran tetramethylrhodamine; Invitrogen) and fluorogold (Fluorochrome, LLC; Denver, CO) retrograde axonal tracers were injected unilaterally into 1 hemi-diaphragm muscle and ipsilateral forelimb muscles (deltoid and triceps), respectively (Boulenguez et al., 2007). Injections were conducted during the same surgery as electrode implantation. Because tracers were injected into muscles prior to the commencement of stimulation, the tracing evaluated the degree of motor neuron loss (but not denervation at the neuromuscular junction) following stimulation. Following laparotomy, 30 µL of fluororuby (10% solution in 2% DMSO/sterile saline vehicle) was injected into 1 hemi-diaphragm (8–10 injection sites per muscle) using a 10 µL Hamilton syringe with an attached 33-gauge needle (45° bevel). For delivery of fluorogold (2.5% solution in dH<sub>2</sub>O vehicle), the ipsilateral forelimb was shaved, and a midline incision in the skin was made on the lateral surface of the limb from the elbow to the shoulder. 75 µL of solution was injected throughout the deltoid and triceps muscles (5 µL per site) using a 10 µL Hamilton syringe with an attached 33-gauge needle (30° bevel). Skin was stapled following forelimb injections.

Three groups of rats were injected with both tracers in identical fashion at the same age (stimulated wild-type, unstimulated SOD1<sup>G93A</sup>, and stimulated SOD1<sup>G93A</sup>), and all rats were sacrificed at the same age (following 9 weeks of stimulation). Briefly, sagittal sections of the entire cervical spinal cord and the rostral part of thoracic spinal cord were cut free-floating at 30 µm thickness. Slices were washed in 0.1 M TBS, mounted on slides, allowed to dry for 2 h, dehydrated through a series of alcohols, and cover-slipped with DPX. Total numbers of fluororuby<sup>+</sup> and fluorogold<sup>+</sup> motor neurons were counted in all sections. In order to rule out the possibility of lost motor neuron labeling (or substantially decreased fluorescent signal below detection levels) at long time points following tracer injection, unstimulated wild-type rats were injected with both fluororuby and fluorogold using the same protocol as described above and were sacrificed at an early time point of 14 days.

### Statistical analysis

Kaplan–Meier analysis of the SOD1<sup>G93A</sup> rats was conducted using the statistical software Sigmaplot (SAS Software) to analyze animal survival. Weight results were analyzed via ANOVA. In all other analyses, Student *t*-test was performed to compare data between groups of animals. All data are presented as mean ± S.E.M., and significance level was set at *p* ≤ 0.05.

## Results

### Development of phrenic nerve stimulation technique in wild-type rats and in the SOD1<sup>G93A</sup> rat model of ALS

We first sought to develop the technique of intra-diaphragm electrode implantation at phrenic motor endpoints for stimulation in wild-type (WT) and SOD1<sup>G93A</sup> rats (see diagram: Fig. 1A). In these initial experiments, we bilaterally implanted both male and female WT and SOD1<sup>G93A</sup> rats with intra-diaphragm electrodes successfully in both hemi-diaphragms at phrenic motor endpoints via laparotomy. All WT (*n* = 4) and SOD1<sup>G93A</sup> (*n* = 6) rats survived surgery and implantation. Peripheral stimulation of phrenic nerves with resulting diaphragm muscle contraction bilaterally was successfully carried out on awake, freely behaving WT and SOD1<sup>G93A</sup> rats, resulting in consistent bilateral contractions of both hemi-diaphragms upon external stimulation. Stimulation at high parameters (see [Materials and methods](#) section for details) could be continued chronically for at least 8 weeks post-implantation in all WT and SOD1<sup>G93A</sup> rats. During the first week post-implantation, rats were subjected to only 30 min of continuous stimulation per day for 3 days a week to allow for accommodation to the prescribed intervention. During weeks 2 and 3, rats received 3 days of stimulation for 2 h per day. Over the remainder of the study, we increased the stimulation regimen to 2 h per day for 5 days a week. Rats were able to tolerate the stimulation without any apparent signs of pain or discomfort during daily stimulation. Furthermore, all electrodes remained in place, and bilateral stimulation consistently resulted in contractions of both hemi-diaphragms, even up to 8 weeks post-implantation. Stimulation never resulted in adverse events such as diaphragm tissue necrosis, animal infection or sudden death. These results demonstrate that intra-diaphragm electrode implantation and subsequent external phrenic nerve motor endpoint stimulation: 1) is feasible, 2) functions in successfully obtaining robust and consistent bilateral diaphragm muscle contraction, and 3) is well tolerated by both WT and SOD1<sup>G93A</sup> rats for extended durations of time.

To examine whether diaphragm stimulation via intramuscular electrode implantation resulted in ectopic stimulation of other motor neuron groups besides phrenic motor neurons, we performed c-Fos labeling of specific populations of motor neurons in the cervical spinal cord. Forelimb motor neurons and phrenic motor neurons were

retrogradely labeled with the fluorescent tracers, fluorogold (FG) and fluororuby (FR), respectively, to allow for identification of specific motor neuron populations. Two weeks later, animals received 2 h of bilateral phrenic nerve stimulation, and were sacrificed 1.5 h following stimulation. Spinal cord sections were immunolabeled with c-Fos. c-Fos expression was detected in scattered FR-labeled phrenic motor neurons (Fig. 1B), but not in FG-labeled forelimb motor neurons (Fig. 1C), suggesting that phrenic nerve stimulation activated phrenic motor neurons, but not forelimb motor neurons.

To also rule out the possibility of ectopic stimulation of motor neurons/muscle groups (besides phrenic nerve/diaphragm), we performed a comprehensive series of intramuscular needle EMG and muscle surface EMG recordings during unilateral phrenic nerve stimulation of SOD1<sup>G93A</sup> rats. Surface EMG recordings of the diaphragm at the costophrenic interface demonstrate electrical activity in ipsilateral diaphragm muscle during stimulation

(Fig. 1D). The recordings displayed in Fig. 1 do not represent motor unit potentials from diaphragmatic contraction but rather demonstrate stimulation from the adjacent electrode. During recording from intramuscular diaphragmatic electrodes, robust intramuscular activity (~3.5 mV) was obtained in the ipsilateral hemi-diaphragm (Fig. 1E), while less activity (~1.0 mV) was also noted in the hemi-diaphragm contralateral to the site of stimulation (Fig. 1F). On the contrary, significant electrical activity during phrenic nerve stimulation was not found with intramuscular needle EMG recordings in the ipsilateral biceps (Fig. 1G), contralateral biceps (not shown), ipsilateral hindfoot (Fig. 1H) or base of tail (not shown). A similar pattern was also found with surface EMG recordings of these same muscles during phrenic stimulation (not shown). In addition, only diaphragmatic contraction (ipsilaterally more than contralaterally) was noted. We did not visually observe muscle contraction in either forelimb or hindlimb muscles. These results demonstrate that phrenic

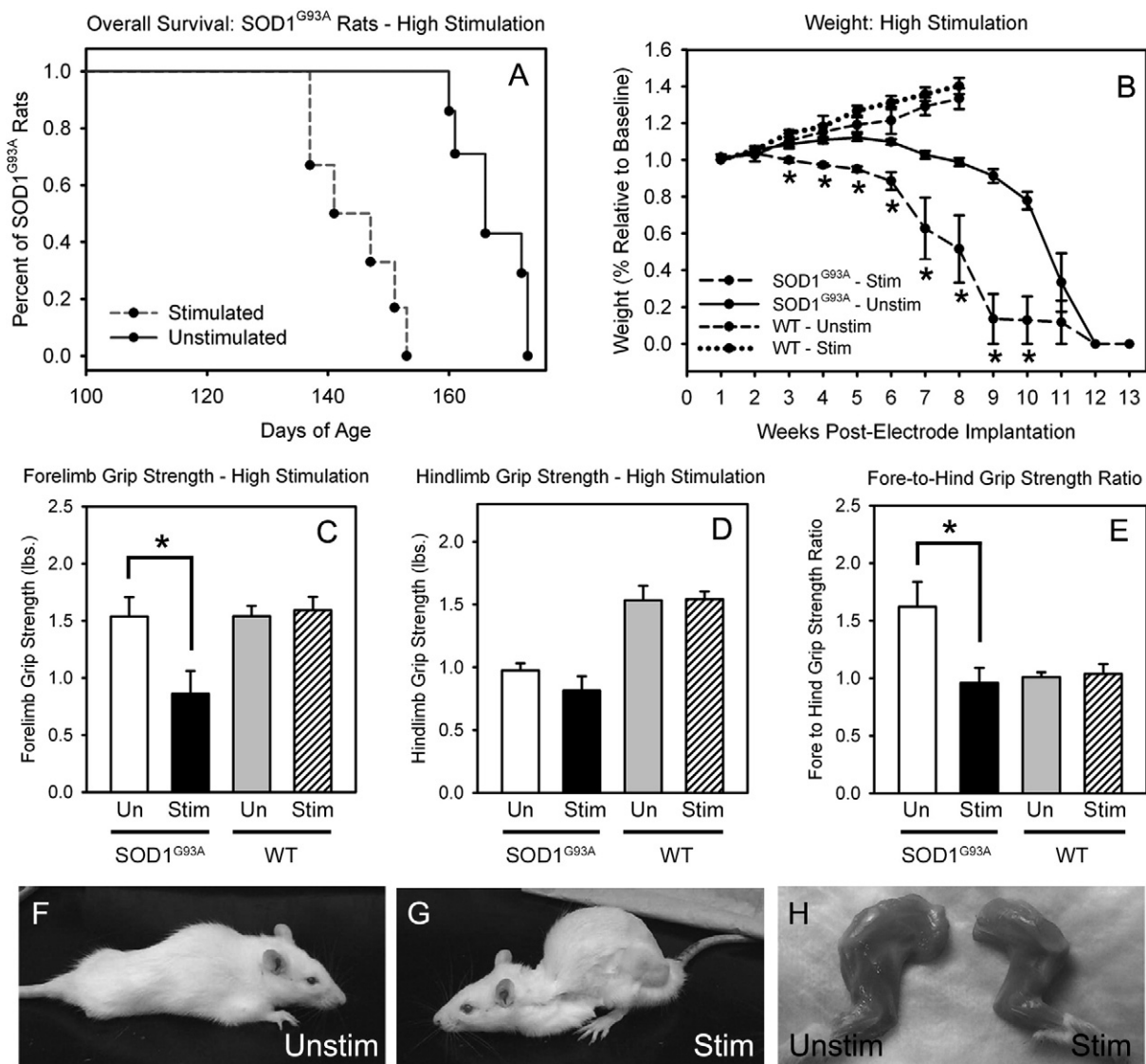


**Fig. 2.** Phrenic nerve hyperstimulation accelerated disease in SOD1<sup>G93A</sup> rats: Bilateral phrenic nerve stimulation at high parameter settings accelerated death in SOD1<sup>G93A</sup> rats by 24 days (A) and weight decline (B) compared to unstimulated SOD1<sup>G93A</sup> rat controls. Compared to unstimulated SOD1<sup>G93A</sup> controls, stimulated SOD1<sup>G93A</sup> rats had significantly reduced forelimb grip strength at 141 days of age (C). No differences in hindlimb grip strength were noted between groups at this same age (D). The ratio of fore-to-hindlimb grip strength is significantly decreased in stimulated SOD1<sup>G93A</sup> rats (E). Therefore, selective phrenic nerve motor point stimulation selectively accelerated decline in forelimb, but not hindlimb, grip strength. This phenotype can be appreciated by comparing representative images of unstimulated (F) and stimulated (G) SOD1<sup>G93A</sup> litter mates. Forelimb muscle atrophy was also accelerated in hyperstimulated SOD1<sup>G93A</sup> rats (H). Unlike SOD1<sup>G93A</sup> rats, bilateral phrenic nerve stimulation in wild-type rats at high parameter settings had no effect on the rate of weight decline at all time points (B) or on forelimb grip strength (C), hindlimb grip strength (D) and fore-to-hindlimb grip strength ratio (E).

nerve stimulation resulted in a regionally (ipsilateral diaphragm) concentrated stimulus. We also conducted needle EMG recordings in the left biceps (Fig. 1I) and left hindfoot (Fig. 1J) during bilateral phrenic nerve stimulation, and did not observe significant electrical activity.

*Phrenic nerve hyperstimulation shortened life span and accelerated weight loss and decline in forelimb motor performance in SOD1<sup>G93A</sup> rats*

The effects of phrenic nerve motor endpoint stimulation were next examined in SOD1<sup>G93A</sup> rats. Ninety-day-old SOD1<sup>G93A</sup> rats were implanted bilaterally, and caged individually to avoid removal of electrodes. Half of the SOD1<sup>G93A</sup> rats received high stimulation 5 days per week for 2 h per day until disease endstage ( $n=7$ ), and the other half of the rats with electrode implants in place for the duration of the study did not receive stimulation and are referred to as “unstimulated: unstim” ( $n=7$ ). Stimulation at high parameter settings (see Materials and methods for description), a stimulation paradigm previously noted to cause neuromuscular fatigue in canine models (Oda et al., 1981), accelerated death by 24 days (unstim:  $167.30 \pm 2.12$  days; stim:  $144.30 \pm 2.91$ ;  $p<0.0001$ ; Fig. 2A) and hastened weight decline ( $p<0.01$  at a number of time points; Fig. 2B) compared to unstimulated controls.

It is important to note that phrenic nerve stimulation did not result in immediate death of stimulated rats. On the contrary, the SOD1<sup>G93A</sup> rats were stimulated for at least 2–3 months before reaching endstage. Similar to sham unstimulated rats, the stimulated animals reached endstage over a range of ages, except that their survival curve was significantly shifted towards earlier ages. In addition, these animals did not quickly reach endstage once they developed disease onset in the forelimbs. Instead, the animals proceeded through a typical progression of increasing limb weakness before succumbing to disease. These

findings show that stimulation accelerated the natural course of disease, but did not result in acute electrical injury to motor neurons. We did not appreciate any muscle tissue necrosis or inflammation at the site of stimulation in the diaphragm (electrode implantation site) to account for reduced respiratory parameters (not shown).

Interestingly, phrenic nerve hyperstimulation selectively accelerated loss of other behavioral functions associated with cervical spinal cord function. Compared to unstimulated sham SOD1<sup>G93A</sup> rats, stimulated SOD1<sup>G93A</sup> rats had significantly reduced forelimb grip strength at 141 days of age (unstim:  $1.54 \pm 0.17$  lbs. of force; stim:  $0.86 \pm 0.20$ ;  $p<0.05$ ; Fig. 2C). However, no differences in hindlimb grip strength were noted between groups at this same age (unstim:  $0.97 \pm 0.06$ ; stim:  $0.81 \pm 0.11$ ;  $p>0.05$ ; Fig. 2D). The typical phenotype in this model results in SOD1<sup>G93A</sup> rats developing weakness first in hindlimb function, followed by development of forelimb weakness, as we have described previously (Howland et al., 2002; Lepore et al., 2008). By expressing fore- and hindlimb grip strength as a ratio of fore-to-hind function, our data suggest that forelimbs retain greater grip strength than the hindlimbs at 141 days of age in unstimulated sham SOD1<sup>G93A</sup> rats. This ratio is significantly decreased in stimulated rats (unstim:  $1.62 \pm 0.22$ ; stim:  $0.96 \pm 0.13$ ;  $p<0.05$ ; Fig. 2E), suggesting that selective phrenic nerve motor endpoint stimulation focally accelerated decline in forelimb, but not hindlimb, grip strength. This reproducible phenotype of forelimb weakness and kyphosis can be appreciated by comparing representative images of unstimulated (Fig. 2F) and stimulated (Fig. 2G) animals. Furthermore, forelimb muscle atrophy was accelerated in hyperstimulated SOD1<sup>G93A</sup> rats (Fig. 2H). These results show that hyperstimulation of vulnerable SOD1<sup>G93A</sup> phrenic nerves in these animals resulted in acceleration of disease progression, including hastened animal death, and altered the phenotype from a predominantly hindlimb onset to a forelimb disease onset.

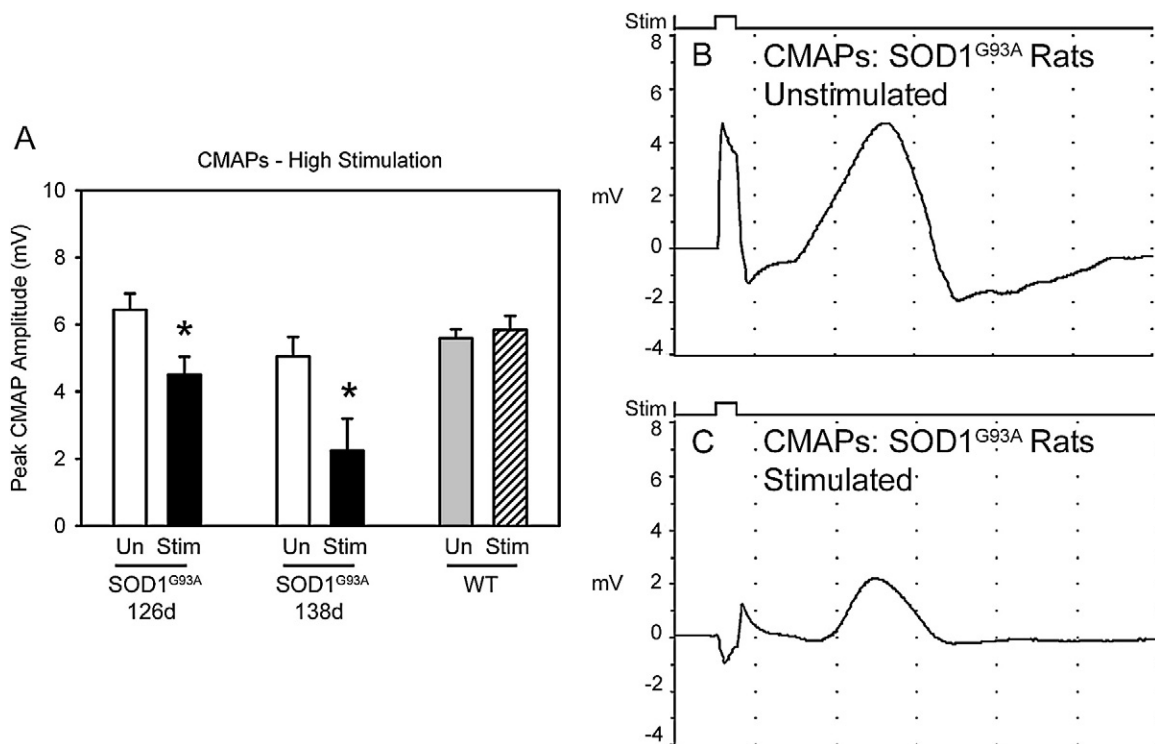


**Fig. 3.** Phrenic nerve hyperstimulation accelerated decline in phrenic nerve compound muscle action potentials (CMAPs) in SOD1<sup>G93A</sup> rats. Compared to unstimulated SOD1<sup>G93A</sup> rats (B), SOD1<sup>G93A</sup> rats that received high stimulation (C) had reduced phrenic nerve compound muscle action potentials (CMAPs), a functional electrophysiological assay of diaphragm function. CMAPs were recorded at 2 different points during disease progression, and a significant decrease in peak response amplitude was found in stimulated rats at both times (A). No effects of high stimulation on CMAP amplitude was noted in wild-type rats (A).

*Phrenic nerve hyperstimulation accelerated decline in phrenic nerve compound muscle action potentials (CMAPs)*

Compared to unstimulated SOD1<sup>G93A</sup> rats (Fig. 3B), SOD1<sup>G93A</sup> rats that received high stimulation (Fig. 3C) had reduced phrenic nerve compound muscle action potentials (CMAPs), a functional electrophysiological assessment of diaphragm function (Llado et al., 2006). CMAPs were recorded at 2 different points during disease progression, and a significant decrease in peak response amplitude was found in stimulated rats at both times (unstim - 126 days:  $6.44 \pm 0.49$  mV; unstim - 138 days:  $5.05 \pm 0.58$ ; stim - 126 days:  $4.5 \pm 0.54$ ; stim - 138 days:  $2.25 \pm 0.95$ ;  $p < 0.05$  at both time points; Fig. 3A). Stimulation had no effect on latency of response (unstim - 126 days of age:  $2.70 \pm 0.07$  ms; unstim - 138 days:  $3.61 \pm 0.21$ ; stim - 126 days:  $2.85 \pm 0.16$ ; stim - 138 days:  $4.08 \pm 0.24$ ;  $p > 0.05$  at both time points; data not shown).

*Phrenic nerve hyperstimulation accelerated loss of cervical spinal cord motor neurons in SOD1<sup>G93A</sup> rats*

Unstimulated SOD1<sup>G93A</sup> rats had significantly greater numbers of total cervical motor neurons at disease endstage than SOD1<sup>G93A</sup> rats

that received high stimulation (unstimulated:  $17.10 \pm 1.02$  motor neurons/section; stimulated:  $10.15 \pm 1.86$ ;  $p < 0.05$ ; Fig. 4A).

To selectively examine the loss of specific motor neuron populations, phrenic motor neurons were retrogradely labeled with the fluorescent tracer, fluororuby (FR), via intramuscular injections into ipsilateral hemi-diaphragm (Fig. 4C). Forelimb motor neurons in the same animals were retrogradely labeled with a second fluorescent tracer, fluorogold (FG), via unilateral intramuscular injections into triceps and deltoid muscles (Fig. 4D). Within cervical spinal cord ventral horn (~C4–C5), phrenic motor neurons and motor neurons innervating the ipsilateral forelimb were in close proximity (Fig. 4B). Compared to wild-type rats that received phrenic nerve hyperstimulation ( $33.3 \pm 14.9$  FR<sup>+</sup> motor neurons/animal;  $210.5 \pm 39.5$  FG<sup>+</sup> motor neurons/animal), both SOD1<sup>G93A</sup> high stimulated ( $5.6 \pm 0.3$  FR<sup>+</sup>;  $49.3 \pm 19.3$  FG<sup>+</sup>) and SOD1<sup>G93A</sup> unstimulated ( $19.6 \pm 16.4$  FR<sup>+</sup>;  $75.0 \pm 27.0$  FG<sup>+</sup>) rats had significantly reduced numbers of forelimb (Fig. 4E) and phrenic (Fig. 4F) motor neurons ( $p < 0.05$ ). In addition, the numbers of forelimb and phrenic motor neurons in the stimulated SOD1<sup>G93A</sup> rats showed a trend towards a reduction when compared to age-matched unstimulated SOD1<sup>G93A</sup> rats ( $p = 0.06$  for phrenic). This suggests that phrenic nerve hyperstimulation accelerated loss of motor neurons (particularly phrenic motor neurons) within the cervical

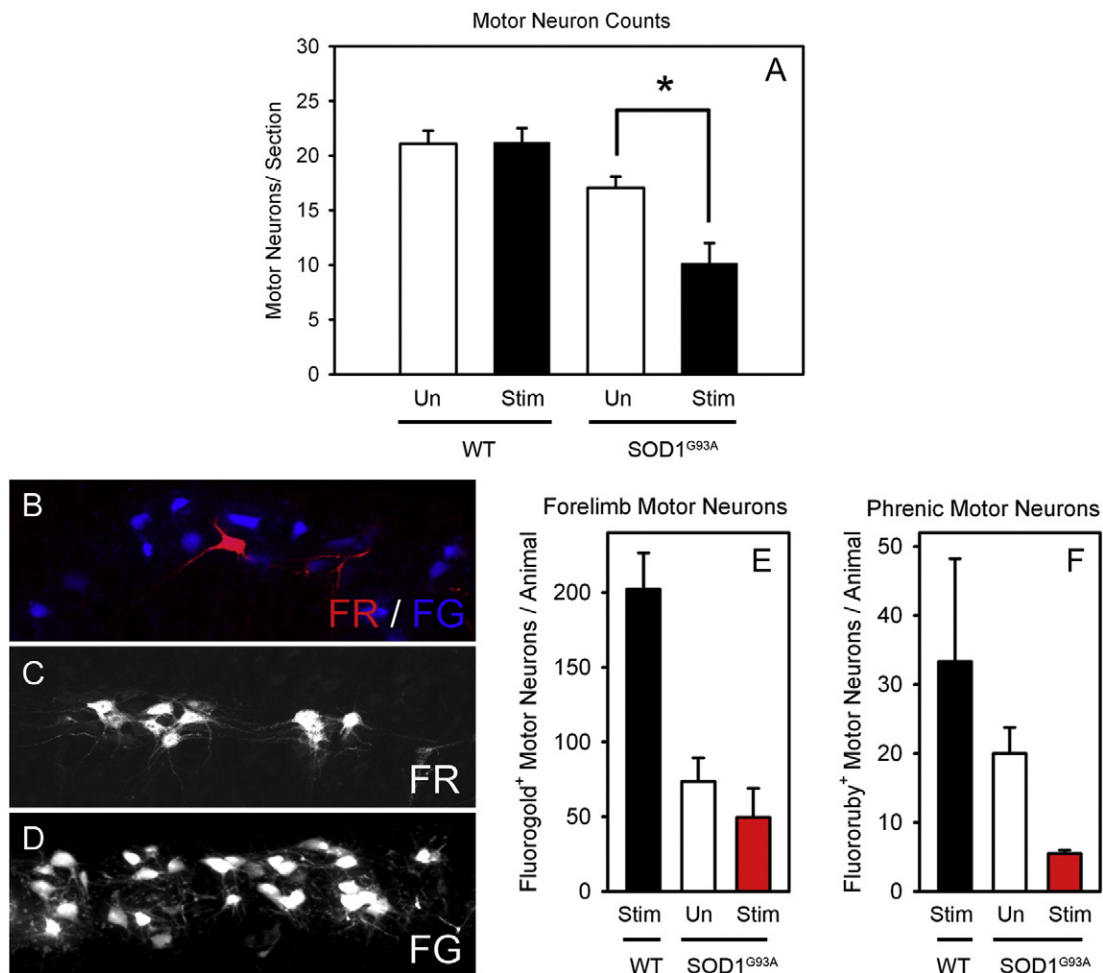


**Fig. 4.** Phrenic nerve hyperstimulation accelerated the loss of both phrenic motor neurons and forelimb motor neurons in SOD1<sup>G93A</sup> rats. Unstimulated SOD1<sup>G93A</sup> rats had significantly greater numbers of cervical motor neurons at disease endstage than SOD1<sup>G93A</sup> rats that received hyperstimulation (A). On the contrary, hyperstimulation of wild-type rats had no effects on numbers of cervical motor neurons (A). Within cervical spinal cord ventral horn (~C4–C5), phrenic motor neurons (fluororuby-labeled; red; C) and motor neurons innervating the ipsilateral forelimb (fluorogold-labeled; blue; D) were in close proximity (B). Compared to wild-type rats that received phrenic nerve hyperstimulation, both SOD1<sup>G93A</sup> stimulated and SOD1<sup>G93A</sup> unstimulated rats had significantly reduced numbers of forelimb (E) and phrenic (F) motor neurons. The numbers of phrenic and forelimb motor neurons in the stimulated SOD1<sup>G93A</sup> rats showed a reduced trend compared to age-matched unstimulated SOD1<sup>G93A</sup> rats.



spinal cord. It is important to note that tracer injections were conducted during the same surgery as electrode implantation. Because tracers were injected into muscles prior to the commencement of stimulation, the tracing evaluated the degree of motor neuron loss (but not denervation at the neuromuscular junction) following stimulation.

To rule out the possibility of lost motor neuron labeling (or substantial decrease in fluorescence signal below detection levels) at long time points, unstimulated wild-type rats ( $n = 3$ ) were sacrificed at 14 days following fluororuby and fluorogold injections to compare the efficiency of motor neuron labeling shortly after injection with

much longer time points. No significant differences were found between motor neuron counts in unstimulated wild-type rats at 14 days ( $33.0 \pm 10.3$  FR<sup>+</sup> motor neurons/animal;  $183.3 \pm 23.3$  FG<sup>+</sup> motor neurons/animal) and 9 weeks (see data above) post-injection, demonstrating that both tracers persist within labeled motor neurons even at long time points.

#### Phrenic nerve hyperstimulation had no effect on wild-type rats

To test if the effects of bilateral phrenic nerve hyperstimulation were specific to vulnerable motor neurons in the neurodegenerative

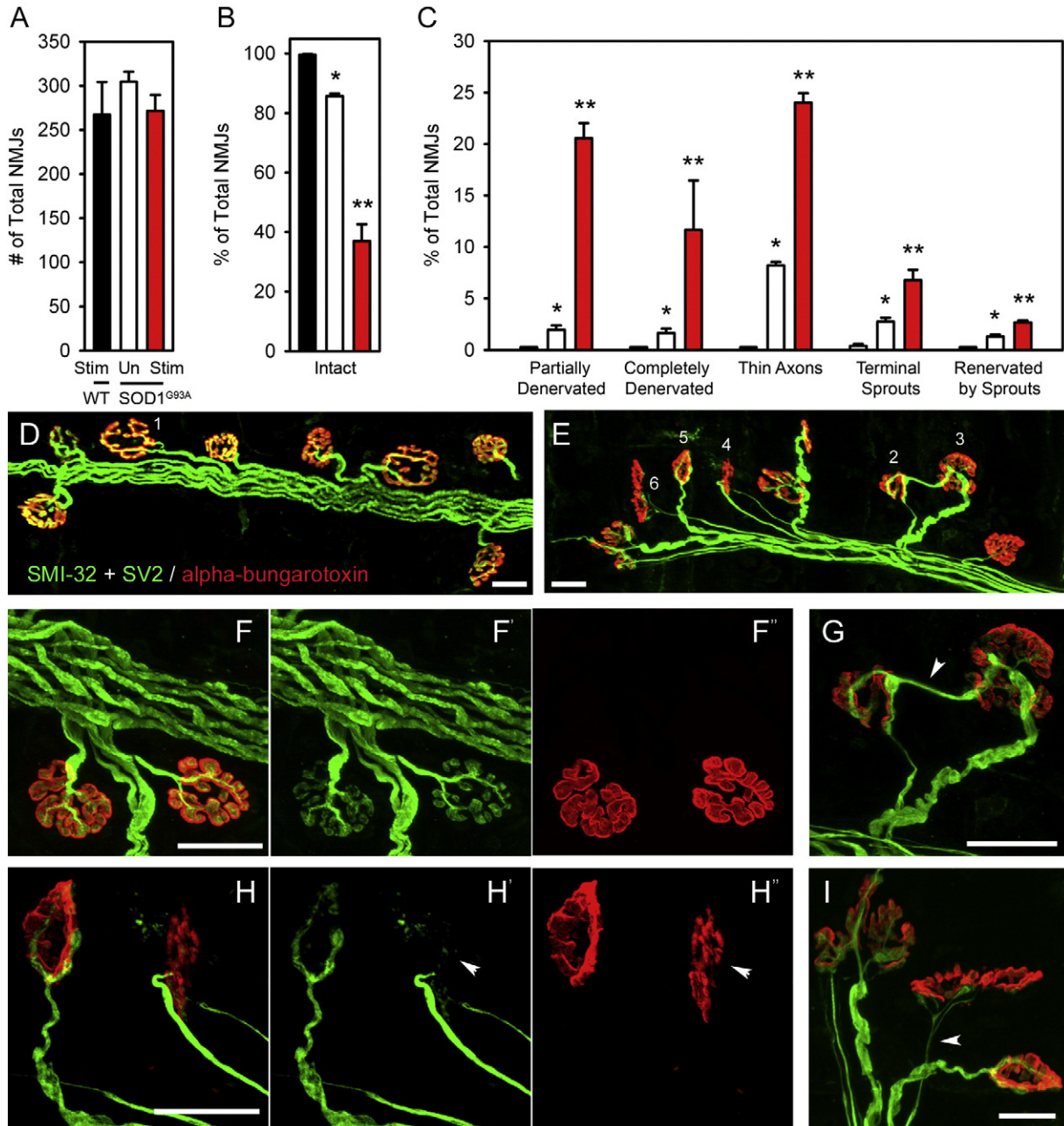


**Fig. 5.** Phrenic nerve hyperstimulation stimulation accelerated pathological changes at diaphragm neuromuscular junctions in SOD1<sup>G93A</sup> rats. There were no differences in total numbers of NMJs among any groups, as assessed by total numbers of alpha-bungarotoxin<sup>+</sup> junctions (A). Nearly all wild-type NMJs were completely intact, characterized by: complete overlap of the pre-synaptic axon and pre-synaptic vesicles with post-synaptic acetylcholine receptors, no signs of multiple innervation, absence of pre-synaptic axon thinning (D: NMJ #1, F). While both groups of SOD1<sup>G93A</sup> rats showed signs of synaptic disruption, stimulated SOD1<sup>G93A</sup> rats had significantly fewer intact junctions, with greater than 60% of junctions being affected (B, E). To specifically examine the types of changes occurring in stimulated diaphragm muscle, NMJ changes were broken down into a number of phenotypic categories. Compared to unstimulated SOD1<sup>G93A</sup> rats, a significantly greater percentage of junctions from stimulated SOD1<sup>G93A</sup> rats showed signs of partial denervation (C, E: NMJ #4 and #5, H - arrowhead), complete denervation (C), thinning of the pre-synaptic axon (C, E: NMJ #6, I - arrowhead), terminal sprouting (C, E: NMJ #3, G - arrowhead) and reinnervation of denervated junctions by terminal sprouts from adjacent junctions (C, E: NMJ #2, G). In many instances, individual junctions showed signs of more than 1 change. Only rare instances of any of these junctional pathologies were found in wild-type stimulated muscles. Scale bars: 25  $\mu$ m.

SOD1<sup>G93A</sup> model, WT rats ( $n = 4$  unstim;  $n = 4$  stim) were subjected to the same stimulation paradigm as SOD1<sup>G93A</sup> rats, including stimulation parameters, age of animals, and frequency and duration of daily stimulation. Unlike SOD1<sup>G93A</sup> rats, high stimulation had no effect in wild-type rats on the rate of weight decline at all time points ( $p > 0.05$ ; Fig. 2B) or on: forelimb grip strength (unstim:  $1.53 \pm 0.12$  lbs. of force; stim:  $1.54 \pm 0.06$ ;  $p > 0.05$ ; Fig. 2C), hindlimb grip strength (unstim:  $1.54 \pm 0.09$ ; stim:  $1.59 \pm 0.12$ ;  $p > 0.05$ ; Fig. 2D), fore-hind grip strength ratio (unstim:  $1.01 \pm 0.04$ ; stim:  $1.04 \pm 0.08$ ;  $p > 0.05$ ; Fig. 2E), cervical motor neuron loss (unstim:  $21.1 \pm 1.18$  motor neurons/section; stim:  $21.2 \pm 1.32$ ;  $p > 0.05$ ; Fig. 4A), CMAP peak amplitude (unstim:  $5.59 \pm 0.27$  mV; stim:  $5.83 \pm 0.42$ ;  $p > 0.05$ ; Fig. 3A) or latency (unstim:  $3.94 \pm 0.19$  ms; stim:  $3.76 \pm 0.06$ ;  $p > 0.05$ ; data not shown) at 146 days of age.

#### Decreased phrenic nerve stimulation had no effect on SOD1<sup>G93A</sup> rats

To test if the effects of bilateral phrenic nerve hyperstimulation on vulnerable cervical motor neurons in SOD1<sup>G93A</sup> rats are specific to stimulation intensity, a separate cohort of SOD1<sup>G93A</sup> rats was subjected to the same stimulation paradigm that accelerated disease in earlier experiments with SOD1<sup>G93A</sup> rats, except that stimulation intensity (see *Materials and methods* section for specifics of changes) was reduced greater than 10-fold ( $n = 5$  unstim;  $n = 4$  stim). Similar to WT rats that received high stimulation, no effects of low stimulation on SOD1<sup>G93A</sup> rats were found in any outcome measures (data not shown).

#### Phrenic nerve hyperstimulation accelerated pathological changes at the diaphragm neuromuscular junction in SOD1<sup>G93A</sup> rats

Previous studies have demonstrated that alterations at the neuromuscular junction are some of the earliest pathological signs occurring in SOD1 rodent models of ALS (Fischer et al., 2004). To examine whether phrenic nerve hyperstimulation induced pathological changes at diaphragm neuromuscular junctions, hemi-diaphragm muscle was examined from age-matched wild-type stimulated, SOD1<sup>G93A</sup> unstimulated and SOD1<sup>G93A</sup> stimulated rats at a single time point (following 9 weeks of stimulation) prior to symptomatic onset of forelimb and respiratory dysfunction. Specifically, motor axons and their terminals were labeled with SMI-312R and SV2-s, respectively, and post-synaptic acetylcholine receptors were labeled with Alexa Fluor 647-conjugated alpha-bungarotoxin. There were no differences in total numbers of NMJs, as assessed by total numbers of alpha-bungarotoxin<sup>+</sup> junctions (WT-stim:  $267.3 \pm 37.0$  junctions; SOD1<sup>G93A</sup> unstim:  $304.7 \pm 11.2$ ; SOD1<sup>G93A</sup> stim:  $271.7 \pm 17.9$ ;  $p > 0.05$  for all comparisons;  $n = 3$ /group; Fig. 5A). Nearly all wild-type NMJs were completely intact, characterized by: complete overlap of the pre-synaptic axon and pre-synaptic vesicles with post-synaptic acetylcholine receptors, no signs of multiple innervation, absence of pre-synaptic axon thinning (Fig. 5D and F). While both groups of SOD1<sup>G93A</sup> rats showed signs of synaptic disruption, stimulated SOD1<sup>G93A</sup> rats had significantly fewer intact junctions, with greater than 60% of junctions being affected (WT-stim:  $99.5 \pm 0.2\%$ ; SOD1<sup>G93A</sup> unstim:  $85.7 \pm 0.8$ ; SOD1<sup>G93A</sup> stim:  $37.0 \pm 5.6$ ;  $p < 0.05$  for all comparisons; Fig. 5B and E). To specifically examine the types of changes occurring in stimulated diaphragm muscle, NMJ changes were broken down into a number of phenotypic categories. Compared to unstimulated SOD1<sup>G93A</sup> rats, a significantly greater percentage of junctions from stimulated SOD1<sup>G93A</sup> rats showed signs of partial denervation (WT-stim:  $0.0 \pm 0.0\%$ ; SOD1<sup>G93A</sup> unstim:  $2.0 \pm 0.4$ ; SOD1<sup>G93A</sup> stim:  $20.6 \pm 1.4$ ;  $p < 0.05$  for all comparisons; Fig. 5C and H), complete denervation (WT-stim:  $0.0 \pm 0.0\%$ ; SOD1<sup>G93A</sup> unstim:  $1.7 \pm 0.4$ ; SOD1<sup>G93A</sup> stim:  $11.7 \pm 4.8$ ;  $p < 0.05$  for all comparisons; Fig. 5C), thinning of the pre-synaptic axon (WT-stim:  $0.0 \pm 0.0\%$ ; SOD1<sup>G93A</sup> unstim:  $2.8 \pm 0.4$ ; SOD1<sup>G93A</sup> stim:  $6.8 \pm 1.0$ ;  $p < 0.05$  for all comparisons; Fig. 5C and I), terminal sprouting (WT-stim:  $0.4 \pm 0.2$ ;

SOD1<sup>G93A</sup> unstim:  $2.8 \pm 0.4$ ; SOD1<sup>G93A</sup> stim:  $6.8 \pm 1.0$ ;  $p < 0.05$  for all comparisons; Fig. 5C and G) and reinnervation of denervated junctions by terminal sprouts from adjacent junctions (WT-stim:  $0.0 \pm 0.0\%$ ; SOD1<sup>G93A</sup> unstim:  $1.3 \pm 0.2$ ; SOD1<sup>G93A</sup> stim:  $2.7 \pm 0.2$ ;  $p < 0.05$  for all comparisons; Fig. 5C and G). In many instances, individual junctions showed signs of more than 1 change. Very few instances of any of these junctional pathologies were found in wild-type stimulated muscles, in accordance with previous work (Love et al., 2003). These results show that, even at an early point in disease prior to symptomatic onset, external phrenic nerve hyperstimulation induced pathological changes at diaphragm neuromuscular junctions, as well as motor neuron loss. The degree of neuromuscular junction loss was not more significant than motor neuron loss at this point, suggesting that a distal “dying back” process, a phenomenon observed in SOD1<sup>G93A</sup> mouse hindlimbs (Fischer et al., 2004), was not evident at least at this timepoint. However, pathological evaluations at even earlier time points could reveal whether early neuromuscular junction changes preceded motor neuron loss.

In order to address whether these morphological changes were consistent with the natural progression of changes at the NMJ observed in the SOD1<sup>G93A</sup> rat, we performed NMJ analysis of unstimulated endstage SOD1<sup>G93A</sup> rat diaphragm. At endstage, the total numbers of alpha-bungarotoxin<sup>+</sup> junctions were unchanged compared to wild-type stimulated, SOD1<sup>G93A</sup> unstimulated and SOD1<sup>G93A</sup> stimulated rats ( $245.5 \pm 2.5$  total junctions; not shown). Compared to SOD1<sup>G93A</sup> unstimulated and SOD1<sup>G93A</sup> stimulated rats, we observed similar morphological changes in the diaphragm of endstage SOD1<sup>G93A</sup> rats, including signs of partial denervation ( $43.8 \pm 0.6\%$  of junctions; not

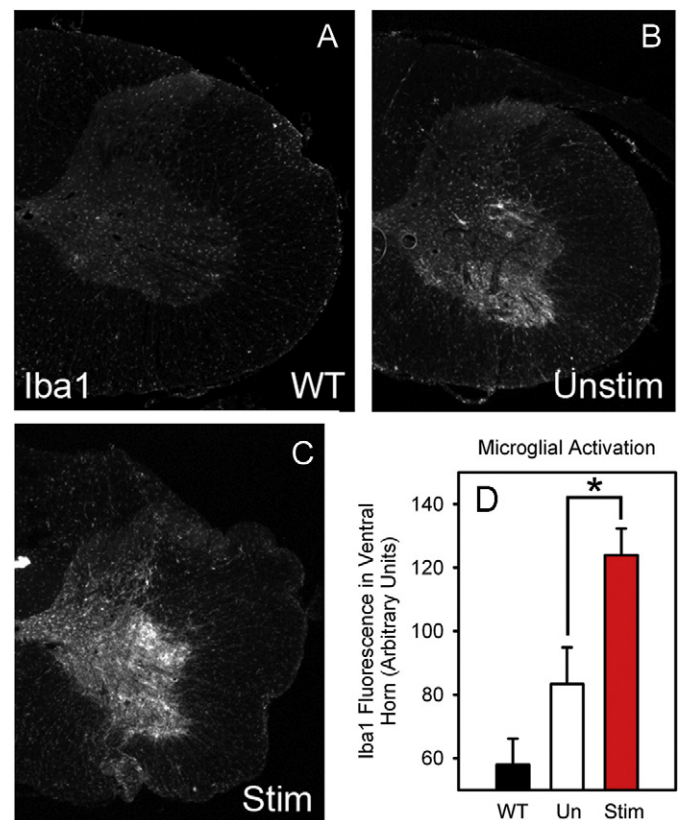


**Fig. 6.** Phrenic nerve hyperstimulation increased cervical spinal cord microgliosis in SOD1<sup>G93A</sup> rats. The inflammatory response was examined with the microglial marker, Iba1, in age-matched cervical spinal cords. Immunohistochemistry revealed that compared to wild-type spinal cord (A), there was a significantly elevated microglial response specifically in the ventral gray matter of both SOD1<sup>G93A</sup> unstimulated (B) and SOD1<sup>G93A</sup> stimulated (C) SOD1<sup>G93A</sup> rat groups. The response was significantly increased in SOD1<sup>G93A</sup> stimulated rats compared to unstimulated SOD1<sup>G93A</sup> animals (D).

shown), complete denervation ( $44.2 \pm 3.0\%$  of junctions; not shown), and thinning of the pre-synaptic axon ( $9.2 \pm 2.7\%$  of junctions; not shown). However, the degree of all of these NMJ pathologies was more pronounced in endstage animals ( $3.0 \pm 0.8\%$  of junctions were completely intact). Therefore, phrenic nerve stimulation accelerated pathological changes at the diaphragm NMJ normally associated with SOD1<sup>G93A</sup> rat disease progression. In addition, stimulation did not induce novel types of NMJ alterations not normally observed in SOD1<sup>G93A</sup>-based disease.

#### *Phrenic nerve hyperstimulation is accompanied by cervical spinal cord microgliosis*

In addition to motor neuron loss, we sought to examine whether other markers of SOD1-mediated disease were active. Microgliosis occurring focally in regions of SOD1<sup>G93A</sup> rat pathology has previously been reported (Lepore et al., 2008). Furthermore, microglial activation has been used in mutant SOD1 mouse models as both a sign of disease activity and a potential contributor to SOD1 disease progression (Boillee et al., 2006; Kriz et al., 2002; Van Den Bosch et al., 2002; Zhu et al., 2002). To examine whether peripheral nerve hyperstimulation resulted in an altered microglial response, Iba1 (a microglial marker) immunostaining was performed in age-matched cervical spinal cords. Immunohistochemistry revealed that compared to wild-type spinal cord (Fig. 6A;  $n = 3$ ), there was a significantly elevated microglial response specifically in the ventral gray matter of both SOD1<sup>G93A</sup> unstimulated ( $n = 3$ ; Fig. 6B) and SOD1<sup>G93A</sup> stimulated ( $n = 3$ ; Fig. 6C) SOD1<sup>G93A</sup> rat groups. However, the response was significantly increased in SOD1<sup>G93A</sup> stimulated rats compared to unstimulated SOD1<sup>G93A</sup> animals (WT-stim:  $57.9 \pm 4.1$  arbitrary units; SOD1<sup>G93A</sup> unstim:  $83.4 \pm 5.7$ ; SOD1<sup>G93A</sup> stim:  $123.9 \pm 4.2$ ;  $p < 0.05$ ;  $n = 3$ /group; Fig. 6D). However, significant differences in GFAP immunostaining between the SOD1<sup>G93A</sup> groups were not prominent (not shown) at the single time point evaluated.

## Discussion

#### *Phrenic motor neuron vulnerability*

Previous electrophysiological and pathological studies have demonstrated that respiratory function in the SOD1<sup>G93A</sup> rat is temporally associated with disease progression, cervical motor neuron loss, and distal denervation (Llado et al., 2006). These data suggest that SOD1<sup>G93A</sup> respiratory pathobiology models human ALS respiratory dysfunction. Furthermore, using cell-transplantation studies, focal neuroprotective effects on motor neurons in this region have resulted in the maintenance of respiratory physiology, prolongation of forelimb strength, and prolonged survival in this model (Lepore et al., 2008). Taken together, our current study suggests that the focal decline in phrenic CMAPs, loss of phrenic motor neurons and distal phrenic denervation, coupled with the sparing of hindlimb grip strength, is likely responsible for the acceleration in stimulated SOD1<sup>G93A</sup> rat death, rather than non-specific systemic effects of this paradigm.

In addition to focal loss of cervical phrenic motor neurons, we also report a significant pathological effect of hyperstimulation at diaphragm neuromuscular junctions (NMJ), including accelerated denervation, axonal thinning and terminal sprouting. Previous work has demonstrated that distal changes at the NMJ can precede actual motor neuron loss in models of ALS (Fischer et al., 2004). It is intriguing to hypothesize that phrenic nerve-diaphragm hyperstimulation in SOD1<sup>G93A</sup> rats worsens disease by accelerating a distal motor neuropathy at the NMJ. However, we also find elevated central motor neuron death at the same time point examined for NMJ changes. Whether a distal motor neuropathy is the first, very early feature in this paradigm is not known since earlier time points following initiation of the experimental paradigm were not

evaluated. Nevertheless, at the time point examined, both motor neuron loss and distal denervation are seen. What is evident in the assessment of distal axons and neuromuscular junctions is that hyperstimulated phrenic motor neurons and their axons in SOD1<sup>G93A</sup> rats are more vulnerable than wild-type motor neurons and that this vulnerability can be induced by activity at the nerve-muscle junction.

#### *Mechanisms and temporal course of disease onset in ALS*

Prevailing evidence suggests that, at least for sporadic ALS, there is no unifying hypothesis for the cause of disease development. However, it is clear that there are unique presentations, including most generally spinal- or bulbar-onset ALS (Mitsumoto et al., 1998). Interestingly, even within groups of patients with familial ALS and/or identical gene mutations, variability in site of onset and disease progression occurs (Andersen et al., 1997; Cudkovic et al., 1997; Mitsumoto et al., 1998). Small reports of ALS following traumatic injury to the peripheral nervous system with onset in a particular associated limb have been published. However, the heterogeneity of the ALS population, as well as an appreciation for the severity of the injury and the time course between injury and development of clinical symptoms, has made such relationships difficult to interpret. Some epidemiological evidence also points to a relationship between developing ALS and environmental factors such as traumatic insult (Kurtzke, 1991), electrical shock (Jafari et al., 2001), military service (Haley, 2003; Horner et al., 2003), and physically fit lifestyles, although methodologies make these small observations difficult to interpret (Armon, 2007). Though inconclusive, these small analyses point to a possible role of peripheral nervous system injury or overactivity in the focal onset of ALS and/or in hastening of disease progression. Given that most cases of ALS are not linked to known genetic causes and that familial-linked cases are heterogeneous even within families, the suggestion that environmental insults are modifiers of disease presentation and progression is an appealing concept.

Motor neurons are particularly vulnerable to cellular insult in ALS. While a number of studies in mouse models of the disease have demonstrated a beneficial effect (or at least a lack of deleterious effects) of moderate exercise on disease parameters (Chen et al., 2008; Kirkinetzos et al., 2003; Liebetanz et al., 2004; McCrate and Kaspar, 2008; Veldink et al., 2003), other studies have also shown that intense exercise paradigms can actually accelerate disease (Mahoney et al., 2004). This threshold effect was observed in the present study. Hyperstimulation of SOD1<sup>G93A</sup> rats via a paradigm that bilaterally activates the phrenic nerves resulted in focal onset of respiratory dysfunction, involvement of adjacent forelimb function and overall accelerated disease progression, while stimulation at a reduced charge density in a separate cohort of SOD1<sup>G93A</sup> rats did not worsen disease. Also, hyperstimulation of wild-type rats did not have these effects, demonstrating a selective vulnerability of motor neurons with a genetic predisposition (SOD1<sup>G93A</sup> mutation) to a high intensity focal insult. These data would suggest that focal injury, in the context of a genetic predisposition to motor neuron disease, may alter both the timing and site of disease onset.

Several studies have demonstrated increased vulnerability of motor neurons in SOD1 rodents to peripheral nerve injury, including exacerbated motor neuron loss following facial nerve avulsion (Ikeda et al., 2005) transection (Mariotti et al., 2002) and sciatic nerve crush (Sharp et al., 2005). These findings support the idea that the SOD1 genotype increases motor neuron vulnerability to peripheral stimuli. Interestingly, previous work has also shown that peripheral axotomy (L5 spinal nerve, sciatic nerve) or nerve crush (tibial nerve) of lumbar motor neurons in SOD1<sup>G93A</sup> models slows loss of motor neurons (Franz et al., 2009; Kong and Xu, 1999). A possible explanation for this paradoxical finding, as well as a connection to the present results, is



that axotomy prevented chronic activation of, and consequent focal injury to, these vulnerable motor neurons. Large motor neurons may be especially vulnerable because of their increased somal and axonal volumes, neurofilament content, excitatory input and metabolic requirements.

We report that hyperstimulation elevated microgliosis in the cervical spinal cord of SOD1<sup>G93A</sup> rats, suggesting that this cellular response may be a marker of this focal disease activity. A number of studies have documented elevated levels of microglial factors, including interleukins, TNF, TGF, COX2 and interferons in mouse models of ALS. These factors seem to be increased in abundance and variety as disease progresses (Sargsyan et al., 2005), consistent with the hypothesis that these cells and their factors are part of a cascade following initial injury. Conversely, administration of minocycline to transgenic mutant SOD1 mice resulted in reduction in microglial activation and prolonged survival (Kriz et al., 2002; Van Den Bosch et al., 2002; Zhu et al., 2002). While microgliosis and other factors may account for the loss of both phrenic motor neurons and adjacent forelimb motor neurons, it is also possible in our experimental paradigm that the decline in forelimb function may be the result of some spread of electrical stimulation to adjacent forelimb motor neurons, rather than only the targeted phrenic motor neuron populations. Therefore, while recent studies have implicated several cell types in both disease onset (Boillee et al., 2006) and progression (Boillee et al., 2006; Yamanaka et al., 2008), the specific mechanisms resulting in local disease pathology and disease involvement among adjacent motor neuron populations remain to be fully elucidated.

## Conclusions

Even though heterogeneities in timing and site of disease onset are well recognized in ALS, few studies have been conducted to elucidate the mechanisms of these clinical phenomena. This study using the SOD1<sup>G93A</sup> rat focused on the chronic stimulation of the phrenic nerve at the motor endpoint. The results reported demonstrate that such peripheral nervous system stimulation can modify both the temporal and anatomical onset of disease in this ALS model and suggest that focal peripheral nervous system overactivity could influence clinical presentations on a genetically susceptible background. This system lays the framework for studying the mechanisms and specific factors that affect site of ALS disease onset, as well as the temporal course and regional involvement of disease. More detailed studies of focal peripheral injury in a more genetically homogeneous human ALS population (such as patients with identical SOD1 mutations) could reveal the importance of peripheral nervous system effects on anatomical sites and timing of disease onset.

## Disclosure of financial interest

Drs. Ray Onders and Anthony Ignagni have a financial interest and are associated with Synapse Biomedical Inc., which provided the materials and equipment for diaphragm stimulation.

## Acknowledgments

We thank: all members of the Maragakis lab for discussion; Project ALS (NJM) and NIH (F32-NS059155: ACL) for funding.

### Author contributions

A.C.L. designed and conducted the experiments, analyzed the data, prepared the figures, and wrote the manuscript. N.J.M. supervised the project, and participated in designing experiments and writing the manuscript. C.T. and M.C.W. designed and conducted experiments. J. O., B.R. and C.D. conducted experiments. R.P.O. and A.R.I. developed

the tools for phrenic nerve stimulation and provided the equipment for stimulation.

## References

- Andersen, P.M., et al., 1997. Phenotypic heterogeneity in motor neuron disease patients with CuZn-superoxide dismutase mutations in Scandinavia. *Brain* 120 (Pt 10), 1723–1737.
- Armon, C., 2007. Sports and trauma in amyotrophic lateral sclerosis revisited. *J. Neurol. Sci.* 262, 45–53.
- Boillee, S., et al., 2006. Onset and progression in inherited ALS determined by motor neurons and microglia. *Science* 312, 1389–1392.
- Boulenguez, P., et al., 2007. Specific and artifactual labeling in the rat spinal cord and medulla after injection of monosynaptic retrograde tracers into the diaphragm. *Neurosci. Lett.* 417, 206–211.
- Bruijn, L.L., et al., 1997. ALS-linked SOD1 mutant G85R mediates damage to astrocytes and promotes rapidly progressive disease with SOD1-containing inclusions. *Neuron* 18, 327–338.
- Chen, A., et al., 2008. The role of exercise in amyotrophic lateral sclerosis. *Phys. Med. Rehabil. Clin. N. Am.* 19, 545–557.
- Cudkowicz, M.E., et al., 1997. Epidemiology of mutations in superoxide dismutase in amyotrophic lateral sclerosis. *Ann. Neurol.* 41, 210–221.
- Fischer, L.R., et al., 2004. Amyotrophic lateral sclerosis is a distal axonopathy: evidence in mice and man. *Exp. Neurol.* 185, 232–240.
- Franz, C.K., et al., 2009. A conditioning lesion provides selective protection in a rat model of Amyotrophic Lateral Sclerosis. *PLoS ONE* 4, e7357.
- Gurney, M.E., et al., 1994. Motor neuron degeneration in mice that express a human Cu, Zn superoxide dismutase mutation. *Science* 264, 1772–1775.
- Haley, R.W., 2003. Excess incidence of ALS in young Gulf War veterans. *Neurology* 61, 750–756.
- Haverkamp, L.J., et al., 1995. Natural history of amyotrophic lateral sclerosis in a database population. Validation of a scoring system and a model for survival prediction. *Brain* 118 (Pt 3), 707–719.
- Horner, R.D., et al., 2003. Occurrence of amyotrophic lateral sclerosis among Gulf War veterans. *Neurology* 61, 742–749.
- Howland, D.S., et al., 2002. Focal loss of the glutamate transporter EAAT2 in a transgenic rat model of SOD1 mutant-mediated amyotrophic lateral sclerosis (ALS). *Proc. Natl. Acad. Sci. U. S. A.* 99, 1604–1609.
- Ikeda, K., et al., 2005. Motoneuron degeneration after facial nerve avulsion is exacerbated in presymptomatic transgenic rats expressing human mutant Cu/Zn superoxide dismutase. *J. Neurosci. Res.* 82, 63–70.
- Jafari, H., et al., 2001. Motor neuron disease after electric injury. *J. Neurol. Neurosurg. Psychiatry* 71, 265–267.
- Kirkinezos, I.G., et al., 2003. Regular exercise is beneficial to a mouse model of amyotrophic lateral sclerosis. *Ann. Neurol.* 53, 804–807.
- Kong, J., Xu, Z., 1999. Peripheral axotomy slows motoneuron degeneration in a transgenic mouse line expressing mutant SOD1 G93A. *J. Comp. Neurol.* 412, 373–380.
- Kriz, J., et al., 2002. Minocycline slows disease progression in a mouse model of amyotrophic lateral sclerosis. *Neurobiol. Dis.* 10, 268–278.
- Kurtzke, J.F., 1991. Risk factors in amyotrophic lateral sclerosis. *Adv. Neurol.* 56, 245–270.
- Lepore, A.C., et al., 2008. Focal transplantation-based astrocyte replacement is neuroprotective in a model of motor neuron disease. *Nat. Neurosci.* 11, 1294–1301.
- Liebetanz, D., et al., 2004. Extensive exercise is not harmful in amyotrophic lateral sclerosis. *Eur. J. Neurosci.* 20, 3115–3120.
- Llado, J., et al., 2006. Degeneration of respiratory motor neurons in the SOD1 G93A transgenic rat model of ALS. *Neurobiol. Dis.* 21, 110–118.
- Lo Coco, D., et al., 2006. Noninvasive positive-pressure ventilation in ALS: predictors of tolerance and survival. *Neurology* 67, 761–765.
- Love, F.M., et al., 2003. Activity alters muscle reinnervation and terminal sprouting by reducing the number of Schwann cell pathways that grow to link synaptic sites. *J. Neurobiol.* 54, 566–576.
- Mahoney, D.J., et al., 2004. Effects of high-intensity endurance exercise training in the G93A mouse model of amyotrophic lateral sclerosis. *Muscle Nerve* 29, 656–662.
- Mariotti, R., et al., 2002. Altered reaction of facial motoneurons to axonal damage in the presymptomatic phase of a murine model of familial amyotrophic lateral sclerosis. *Neuroscience* 115, 331–335.
- Matsumoto, A., et al., 2006. Disease progression of human SOD1 (G93A) transgenic ALS model rats. *J. Neurosci. Res.* 83, 119–133.
- Mattson, M.P., 2004. Infectious agents and age-related neurodegenerative disorders. *Ageing Res. Rev.* 3, 105–120.
- McCrack, M.E., Kaspar, B.K., 2008. Physical activity and neuroprotection in amyotrophic lateral sclerosis. *Neuromolecular Med.* 10, 108–117.
- Mitsumoto, H., et al., 1998. Amyotrophic lateral sclerosis. F.A. Davis, Philadelphia.
- Nagai, M., et al., 2001. Rats expressing human cytosolic copper-zinc superoxide dismutase transgenes with amyotrophic lateral sclerosis: associated mutations develop motor neuron disease. *J. Neurosci.* 21, 9246–9254.
- Oda, T., et al., 1981. Evaluation of electrical parameters for diaphragm pacing: an experimental study. *J. Surg. Res.* 30, 142–153.
- Ravits, J., Traynor, B.J., 2008. Current and future directions in genomics of amyotrophic lateral sclerosis. *Phys. Med. Rehabil. Clin. N. Am.* 19, 461–477 viii.
- Rosen, D.R., et al., 1993. Mutations in Cu/Zn superoxide dismutase gene are associated with familial amyotrophic lateral sclerosis. *Nature* 362, 59–62.



- Sargsyan, S.A., et al., 2005. Microglia as potential contributors to motor neuron injury in amyotrophic lateral sclerosis. *Glia* 51, 241–253.
- Sharp, P.S., et al., 2005. The effect of peripheral nerve injury on disease progression in the SOD1(G93A) mouse model of amyotrophic lateral sclerosis. *Neuroscience* 130, 897–910.
- Sutedja, N.A., et al., 2008a. What we truly know about occupation as a risk factor for ALS: a critical and systematic review. *Amyotroph Lateral Scler.* 1–19.
- Sutedja, N.A., et al., 2008b. Exposure to chemicals and metals and risk of amyotrophic lateral sclerosis: a systematic review. *Amyotroph Lateral Scler.* 1–20.
- Van Den Bosch, L., et al., 2002. Minocycline delays disease onset and mortality in a transgenic model of ALS. *NeuroReport* 13, 1067–1070.
- Veldink, J.H., et al., 2003. Sexual differences in onset of disease and response to exercise in a transgenic model of ALS. *Neuromuscul. Disord.* 13, 737–743.
- Wong, P.C., et al., 1995. An adverse property of a familial ALS-linked SOD1 mutation causes motor neuron disease characterized by vacuolar degeneration of mitochondria. *Neuron* 14, 1105–1116.
- Wright, M.C., et al., 2007. Distinct patterns of motor nerve terminal sprouting induced by ciliary neurotrophic factor vs. botulinum toxin. *J. Comp. Neurol.* 504, 1–16.
- Yamanaka, K., et al., 2008. Astrocytes as determinants of disease progression in inherited amyotrophic lateral sclerosis. *Nat. Neurosci.* 11, 251–253.
- Zhu, S., et al., 2002. Minocycline inhibits cytochrome c release and delays progression of amyotrophic lateral sclerosis in mice. *Nature* 417, 74–78.